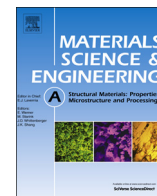




ELSEVIER

Contents lists available at ScienceDirect

## Materials Science &amp; Engineering A

journal homepage: [www.elsevier.com/locate/msea](http://www.elsevier.com/locate/msea)

## Decoupling of the softening processes during rapid tempering of a martensitic steel

Elliot Biro<sup>a,b</sup>, Joseph R. McDermid<sup>c,\*</sup>, Samuel Vignier<sup>a</sup>, Y. Norman Zhou<sup>d</sup><sup>a</sup> ArcelorMittal Global Research, 1390 Burlington Street, Box 2460, Hamilton, Ont., Canada L8N 3J5<sup>b</sup> Department of Materials Science and Engineering, McMaster University, 1280 Main Street West, Hamilton, Ont., Canada L8S 4L8<sup>c</sup> McMaster Steel Research Centre, McMaster University, 1280 Main Street West, Hamilton, Ont., Canada L8S 4L8<sup>d</sup> Department of Mechanical and Mechatronics Engineering, University of Waterloo, 200 University Avenue West, Waterloo, Ont., Canada N2L 3G1

## ARTICLE INFO

## Article history:

Received 2 March 2014

Received in revised form

23 July 2014

Accepted 29 July 2014

Available online 6 August 2014

## Keywords:

Martensite

Tempering

Transformation kinetics

HAZ softening

## ABSTRACT

The increased adoption of martensite-containing advanced high strength steels, such as martensitic and dual-phase steels, into automotive applications has led to concerns among practitioners with respect to softening during rapid tempering cycles such as those experienced during laser welding. Past studies on rapid tempering have successfully modeled the rapid tempering process; however, the activation energies and softening rates calculated did not match the classic literature values associated with martensite tempering. The present study examined rapid tempering data for a martensitic steel and separated the softening process into two stages: carbide nucleation and carbide coarsening or growth. The activation energies calculated for each process were found to be consistent with classic literature values for diffusion controlled nucleation and growth of carbides during martensite tempering.

© 2014 Elsevier B.V. All rights reserved.

## 1. Introduction

Automotive manufacturers are widely required by legislation to improve vehicle fuel economy [1]. Among the solutions being pursued to realize this objective is structural component weight reduction by reducing steel sheet thickness. However, in order to meet structural requirements while reducing material thickness, automakers are replacing lower strength conventional steels with higher strength advanced high strength steel (AHSS) grades such as martensitic, dual-phase (DP) and transformation induced plasticity (TRIP) steels [2].

AHSS derive their high strengths from complex microstructures comprising mixtures of various volume fractions of martensite, ferrite, bainite and retained austenite [3,4]. Although all of these alloys exhibit an excellent strength–ductility balance, they contain phases that decompose at higher temperatures. In automotive assembly, this is observed in the tempered area of weld heat affected zones (HAZ), where martensite and (if present) retained austenite typically decompose during welding and the local hardness and ultimate tensile strength decrease [5,6]. This phenomenon, known as HAZ softening, was first observed in flash-butt wheel rim welding applications [7,8]. Since its initial

characterization, a number of authors have investigated HAZ softening. Some early workers concluded that HAZ softening was a strong function of the length of time the material temperature was elevated [9–11]. In these studies, HAZ softening was reduced by increasing the cooling rate after welding, thereby reducing the overall time the weldment was at an elevated temperature. Further work into this phenomenon has shown that HAZ softening is also related to material chemistry and initial microstructure. For example, the maximum HAZ softening possible in DP steels has been shown to be linearly dependant on martensite volume fraction [12] as the observed hardness decrease was due to martensite decomposition whereas no significant hardness changes were observed in the ferritic matrix [13]. Other authors have shown that HAZ softening kinetics are affected by alloy chemistry. For instance, increasing the martensite C content has been found to increase the softening rate [6]. Conversely, alloying with carbide forming elements (e.g. Cr, Mo) has been shown to slow softening by either retarding cementite precipitation or growth within the tempered martensite [6,14,15].

Limited work has been done on quantifying the effects of thermal history, microstructure and steel chemistry on martensite softening kinetics using rapid heat treatments consistent with those associated with laser welding [16–18]. These studies used a characteristic equation, such as the Johnson–Mehl–Avrami–Kolmogorov (JMAK) equation [19–22], to characterize the softening kinetics. In these cases,

\* Corresponding author.

E-mail address: [mcdermid@mcmaster.ca](mailto:mcdermid@mcmaster.ca) (J.R. McDermid).

Nomenclature			
$b$	Burger's vector length	$k_0$	fitting parameter for $k$
$C_0$	initial concentration of solute atoms in the matrix	$k_1$	geometric constant for grain boundary particle growth
$d$	particle diameter	$L$	inter-particle spacing
$d_0$	particle diameter at initial time $t_0$	$m$	coarsening rate exponent
$D_{gb}$	grain boundary diffusion coefficient	$M_T$	Taylor factor
$D_{gb}^0$	pre-exponential factor for grain boundary diffusion coefficient	$n$	JMAK rate exponent
$D_V$	volumetric diffusion coefficient	$q$	conversion factor from Vickers hardness to yield strength
$D_V^0$	pre-exponential factor for volumetric diffusion coefficient	$Q$	activation energy
$G$	shear modulus	$R$	universal gas constant
$H_{BM}$	as-received base material hardness	$t$	time
$H$	instantaneous material hardness	$t_0$	initial time for particle coarsening equation
$H_\infty$	minimum material hardness	$T$	temperature
$\Delta H$	change in material hardness due to particle coarsening	$V_M$	particle molar volume
$k$	energy barrier to material softening (JMAK equation)	$\delta$	grain boundary width
$k_D$	diffusion dependant constant	$\gamma$	particle surface energy per unit area of interface with matrix
		$\phi$	softening parameter

the softening kinetics were derived from a series of rapid isothermal tempering experiments designed to allow for the calculation of the tempering activation energy and rate exponent. Although these studies did show that transient softening could be quantified and predicted, the derived tempering activation energies and rate constants did not agree with those of the classic martensite tempering literature [16]. As it has been widely reported that martensite tempering is responsible for HAZ softening [6,7,9–11,13,15,16,23], it was expected that the activation energy for the softening process would be approximately 80–123 kJ/mol, the activation energy for C diffusion in ferrite [24,25], and the JMAK exponent would be approximately 0.67, the value associated with the precipitation of particles on dislocations [26]. Instead, the activation energy and rate exponent derived were approximately 28.3 kJ/mol and 0.10, respectively, for the martensitic M220 alloy [16]. Biro et al. [16] suggested that this disagreement was due to several processes being combined within the rapid tempering data, namely: martensite tempering, cementite precipitation and growth, ferrite recrystallization and grain growth. Unfortunately, without a clear understanding of the underlying processes responsible for HAZ softening, this process cannot be modeled or predicted phenomenologically. Thus, the current study will re-examine the data of Biro et al. [16] and expand the previous rapid tempering study for the fully martensitic M220 steel in order to more fully determine and decouple the metallurgical processes responsible for softening during rapid tempering as applied to HAZ softening in advanced steels.

## 2. Experimental methods

All experiments were carried out using an industrially fabricated 1.8 mm thick M220 grade martensitic steel. The as-received microstructure was produced via a continuous annealing line. The M220 chemical composition and as-received hardness can be found in Table 1. Microhardness traverses conducted on the sheet

**Table 1**  
Chemistry (in wt%) and hardness of M220 experimental steel.

C	Mn	P	S	Si	Cr	Mo	Base hardness (HV)	Min hardness (HV)
0.23	0.4	0.01	0.01	0.20	0.02	0.00	478.0	200.0

cross-sections revealed that there were no significant hardness variations across the sheet thick thickness.

All rapid tempering heat treatments were carried out using a Gleeble 3500 (Dynamic Systems Inc., Poestenkill, NY, USA). Samples comprised 100 mm × 12 mm coupons with the rolling direction parallel to the sample long axis. During tempering, average sample heating and cooling rates were approximately 2200 °C/s and 4100 °C/s, respectively. These heating and cooling rates allowed the rapid tempering cycles to be considered isothermal, as verified via a Hollomon-Jaffe analysis [27] of the thermal profiles. Details of this analysis, with sample thermal profiles, are provided in Appendix A. Experimental tempering times and temperatures are listed in Table 2. However, it should be noted that tempering times of 20 s and 50 s were used only for tempering temperatures of 420 °C or less.

All microhardness measurements were made using a Vickers indenter on metallographically prepared sample cross sections. In all cases, a 500 gf load and 15 s dwell time were employed. Testing locations were separated by at least three indentation widths in accordance with ASTM E384-11 [28]. All microhardness data presented are the average of at least 10 measurements taken across the material thickness in order to account for any through-thickness heterogeneity. Error bars on the microhardness measurements represent the 95% confidence interval (CI) of the average microhardness value. In cases where data are presented without visible error bars, the 95% CI was smaller than the size of the plot symbol.

The microstructures of selected samples were examined using optical (OM) and scanning electron microscopy (SEM). In all cases samples were sectioned, mounted, and polished using standard metallographic methods. SEM samples were etched with 2% nital and gold coated before imaging with a JEOL JSM-6460LV SEM (JEOL Ltd., Tokyo, Japan) using an acceleration voltage of 20 keV. Optical microscopy samples were etched with Marshall's reagent. Grain size measurements utilized the linear intercept method [29].

All carbide equivalent diameters were measured from carbon replicas from samples tempered at either 500 °C or 600 °C viewed via transmission electron microscopy (TEM). Replicas were made using standard methods, as described in [6], and were observed using a Philips CM12 TEM (Royal Philips Electronics, Amsterdam, The Netherlands) at an acceleration voltage 120 keV. Carbides were identified manually and their equivalent circular diameter determined using Clemex Vision – Professional Edition ver. 5.0.008e (Longueuil, Quebec, Canada) image analysis software.

Download English Version:

<https://daneshyari.com/en/article/7980168>

Download Persian Version:

<https://daneshyari.com/article/7980168>

[Daneshyari.com](https://daneshyari.com)